J Mater Sci (2008) 43:7409–7417
DOI 10.1007/s10853-008-2724-9

ULTRAFINE-GRAINED MATERIALS

Mechanical properties and corrosion behaviour of ultrafine-grained AA6082 produced by equal-channel angular pressing

Matthias Hockauf · Lothar W. Meyer · Daniela Nickel · Gert Alisch · Thomas Lampke · Bernhard Wielage · Lutz Krüger

Received: 7 March 2008 / Accepted: 12 May 2008 / Published online: 21 July 2008

Abstract The mechanical properties and corrosion behaviour of AA6082 with ultrafine-grained (UFG) microstructure were investigated. The material was processed by equal-channel angular pressing (ECAP) up to eight extrusions at room temperature in a 90°-die with active backpressure. Besides the peak-aged temper, which provides maximum strengths and strongly reduced ductility, the solution heat treated condition was considered as well. Combined with post-ECAP aging, an optimum of high strength, ductility and impact toughness was achieved. The corrosion investigations and the examination of the corrosion damage of the UFG-materials show higher pitting corrosion resistance compared to the unprocessed material. The optimised condition was used for the production of screw prototypes which showed appreciable higher strength and ductility compared to the identically manufactured screws from the CG counterpart. Such materials are potential candidates to be used for several engineering applications such as high strength screws even at higher temperatures.

M. Hockauf (✉) · L. W. Meyer
Institute for Materials and Impact Engineering, Chemnitz University of Technology, Erfenschlager Str. 73, 09125 Chemnitz, Germany
e-mail: matthias.hockauf@mb.tu-chemnitz.de

D. Nickel · G. Alisch · T. Lampke · B. Wielage
Institute for Composite Materials and Surface Technology, Chemnitz University of Technology, Erfenschlager Str. 73, 09125 Chemnitz, Germany

L. Krüger
TU Bergakademie Freiberg, Institute for Materials Engineering, Gustav-Zeuner Straße 5, 09596 Freiberg, Germany

Introduction

Equal-channel angular pressing or -extrusion (ECAP/-E) was originally developed by Segal et al. [1] in the beginning of the 80s in the last century to introduce a homogeneous simple shear deformation into billets without changing its cross section. Since the early 90s, the method was spreading out worldwide and has been improved by many research groups. Currently, ECAP is considered as the most promising method for achieving homogeneous ultrafine-grained (UFG) microstructures with improved properties in many metallic bulk materials [2]. Previous reports provide a detailed description of the microstructural characteristics and the mechanical properties associated with ECAP for Al and Al-alloys [3–6]. Recently, the commercialisation of ECAP was reported by Honeywell [7] for flat Al and Cu billets up to masses of ~33 and ~110 kg, respectively, provided as sputtering targets for electronic applications.

Nevertheless, despite the enormous number of ECAP-related publications only a few practical applications are proposed to date. For example, for applications of magnesium or aluminium alloys in gearboxes and engines, screws made of aluminium alloys offer many advantages when compared to their steel counterparts [8]. These include weight savings and higher connection strengths due to their similar thermal expansion behaviour. Besides the mechanical properties, the susceptibility to corrosion is the most critical factor for the final engineering application of products. However, studies including the corrosion behaviour of SPD materials with UFG microstructure are still rare and their results are contradictory [9]. The first report on this topic dealt with pure UFG Cu (>99.60 wt.%), published in 1999 [10], followed by Ti (>99.36 wt.%) [11] and recently Al (>99.99 wt.%) [12]. In the absence of impurities or

alloying elements forming second phases, the corrosion resistance after ECAP is unchanged [13] or slightly decreased [14]. The morphology after the corrosion tests of UFG Cu appears more homogeneous when ECAP as method for grain refinement is used [13, 14]. The results of [11, 12, 15–17] suggest that UFG metals containing impurities or alloying elements also exhibit an improved corrosion behaviour if compared to the coarse-grained (CG) counterparts.

In this study an optimisation of commercial AA6082 by ECAP combined with subsequent heat treatment is presented, particularly with regard to the mechanical and corrosion properties. The optimised material is used for the production of high-quality screw prototypes with enhanced properties, proposing a new area of engineering application for products with UFG microstructure.

Experimental

For the investigations commercial AA6082 (Al, Si 0.98 wt.%, Mg 0.70 wt.%, Mn 0.58 wt.%, Fe 0.21 wt.%, Cu 0.02 wt.%) with CG was supplied by Hydro Aluminium Deutschland in the form of extruded square bars in peak-aged temper (T6). This condition will be further on referred to as *CG-T6*. After machining the billets to the initial geometry of $15 \times 15 \times 120$ mm^3, multi-pass ECAP processing was done on a first batch of billets in the as supplied CG-T6 condition at room temperature (RT) in a die-set with an angle of 90° between the two intersecting channels, resulting in an equivalent plastic strain of $\sim$1.15 per extrusion. The friction conditions inside the tooling are optimised by two movable walls in the inlet channel and a bottom slider in the outlet channel [18]. The extrusions were done with a constant punch speed of 25 mm min^{-1}, following route E that represents a 180° rotation of the billet about the extrusion axis between pass one and pass two, a 90° clockwise rotation between pass two and pass three, and a 180° rotation between pass three and pass four and so on. In a sense, this hybrid route consists of the commonly used route C [19], with 90° rotations in the same sense after an even number of passes [20]. It combines a rapid break-up of the microstructure with a high fraction of fully worked material inside the billet. To ensure homogeneous plastic flow and to avoid the formation of a corner gap, controlled backpressures up to 100 MPa were applied via the bottom slider. The conditions produced by this approach will be further on referred to as *UFG* together with the processing route and number of extrusions (e.g. *UFG-E2*). Recently, it was shown for AA6060 that both strength and ductility can be improved by either processing at cryogenic temperatures [21–23] or at RT in the solid-solution temper followed by aging at higher temperature [24–29]. It was shown for Al–Mg–Si Al alloys that the effect on ductility is most remarkable after only one single pressing, which makes the process even more attractive for practical applications [27, 29]. Thus, a second batch of AA6082 billets was solid-solution heat treated prior to ECA-pressing at 530 °C for 60 min, followed by quenching into cold water. According to the optimal parameters [29], subsequent post-ECAP aging was performed at 170 °C for 18 min corresponding to the peak hardness in this case. This condition will be further on referred to as *UFG-HT*. For the characterisation of strength and ductility, tensile specimens with an aspect ratio of the gauge length of three were machined from the billets in the direction of extrusion. Quasi-static tensile tests were operated according DIN EN 10002 in a conventional testing machine Zwick-Roell at constant crosshead speed with an initial strain rate of 6×10^{-4} s^{-1}. Specimens for impact toughness testing were machined along the direction of extrusion according the standard DIN 50115. The geometry of the samples was $4 \times 4 \times 44$ mm^3. The V-shaped notch (depth of 1 mm, 45° opening angle, 0.25 mm notch-radius) was machined so that the direction of crack propagation is parallel to the transverse plane (X) towards the flow plane (Y) of the billets, respectively [30]. An instrumented miniature Charpy impact tester with a nominal energy of 15 J was used to measure the absorbed energy (KV). For the fabrication of screw prototypes with metric coarse thread (major diameter = 6 mm, length = 50 mm), flat-die thread rolling was performed by RIBE Verbindungstechnik Schwabach. Consecutively, quasi-static tensile tests were performed on the screws at a constant crosshead speed of 1 mm min^{-1} following DIN EN ISO 898. The gauge length was 24.7 mm, covering $\sim$25 convolutions. For the calculation of stresses, the corresponding tensile stress area of 20.1 mm^2 was used. For the evaluation of all mechanical properties at least three parallel tests of the same condition were performed at RT and typical curves are presented.

The corrosion characteristics were measured in the flow plane (Y) of the billets using an electrochemical workstation IM6 from Zahner-electric with a conventional three-electrode cell-setup. The potentials were measured against the saturated calomel electrode (SCE) with a Haber-Luggin capillary. The platinum plate was used as counter electrode. All measurements of the polished samples (working electrode) were performed in neutral 0.1 M NaCl test solution at 25 °C. Both cyclovoltammetry (CV) for the evaluation of the pitting corrosion resistance and electrochemical impedance spectroscopy (EIS) were applied. For the CV measurements the potential is a swept of 0.625 mV s^{-1} between the anodic and cathodic potential limits. The current is measured and related to the area. Therefore, the experimental curve obtained consists of this current density as a function of the potential and represents a set of cyclic

polarization curves. Before and after each test the surface of the specimen was cleaned with ethanol. Each CV measurement consists of three cycles between −1000 and −600 mV with a resolution of 1 mV. The EIS investigations explore the frequency dependent impedance at open circuit potential with a sinusoidal AC perturbation of 10 mV amplitude, applied over a frequency range from 100 kHz down to 100 mHz. The corrosion potential E_{corr} and the current density i_{corr} were evaluated from the first cycle of the potentiodynamic curves using the Tafel extrapolation procedure. E_{corr} describes the corrosion resistance and i_{corr} the rate of corrosion. The rapid increase of anodic current densities at a given potential is caused by the passive film breakdown and the associated begin of pitting that is defined as pitting corrosion potential E_{pit}. The surface morphology of the samples was examined with a scanning electron microscope LEO 1455 from Carl Zeiss equipped with an energy dispersive X-ray spectrometer (EDXS). Additional investigations were done by scanning transmission electron microscopy (STEM) with the same system. The CV corrosion damage was evaluated and graphically displayed by the Hommel tester T4000 measuring station, using the 3D-topography measurement (recording parameters: travel 4 mm, step width 2.5 μm, 9600 measure points, 5 μm tip radius).

Results and discussion

Mechanical properties

In Fig. 1 the quality of the AA6082 billets before and after ECA-pressing for one, two and eight ECA-extrusions at RT is shown. It is apparent from the shape of the billets that due to the application of moving parts inside of the die a very uniform shear strain is achieved up to high strains. This is benefited by the sharp channel corner and the applied backpressure. The reduction in length (∼2% per extrusion) is caused by the reshaping of the billets due to the elastic expansion of the die during processing. Figure 2 shows the mechanical behaviour for the investigated AA6082 in different conditions. The selected data from quasi-static tensile tests in Fig. 2a reveal the well-known behaviour of a strongly increased strength during the first ECA-pressings (UFG-E2) caused by a rapid multiplication of defects. Further processing results in a lower increase, since accumulation and annihilation of defects is increasingly equalised approaching a saturation level.

After eight extrusions (UFG-E8) an increase of 75% in yield strength and ∼55% in ultimate tensile strength is reached when compared with the CG-T6 material. Since the material gets severely strain hardened during processing, the grain refinement is accompanied to a significant reduction in ductility. Thus, the engineering stress–strain curves peak at very small plastic strains and then drops as the localised deformation promotes necking and fracture. This behaviour is particularly pronounced for low extrusion

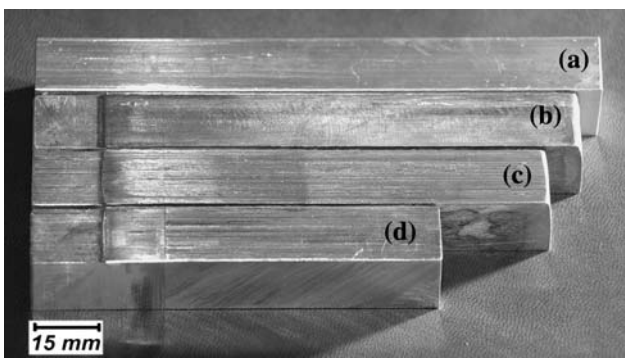

Fig. 1 High-quality billets (**a**) before (15 × 15 × 125 mm^3) and after ECAE for (**b**) one, (**c**) two and (**d**) eight extrusions at RT following route E

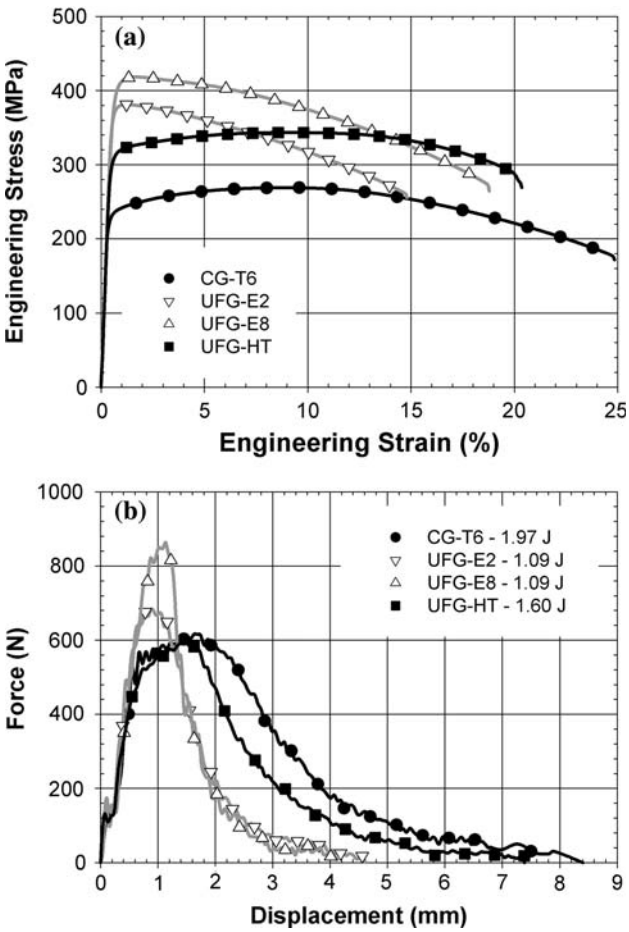

Fig. 2 Mechanical behaviour for the investigated AA6082 in different conditions: (**a**) engineering stress–strain curves from quasi-static tensile tests; (**b**) force–displacement curves received from Charpy impact tests

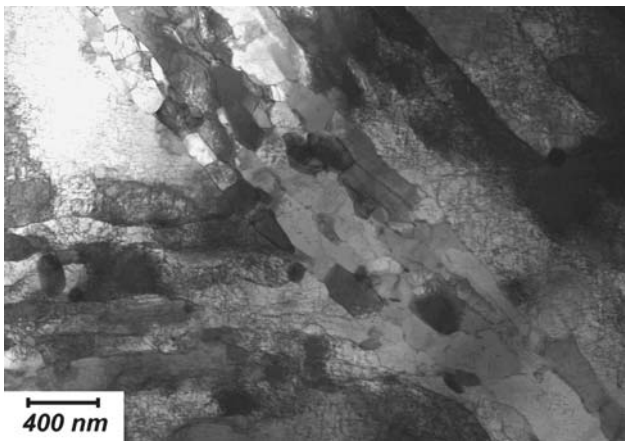

Fig. 3 STEM micrograph representing the microstructure of the optimised condition (UFG-HT) in the flow plane after one extrusion at RT in the solid-solution temper followed by aging at 170 °C for 18 min

numbers (UFG-E2) as discussed in [30]. As shown in [29] for AA6060, the problem of reduced ductility can be overcome by the application of a post-ECAP heat treatment. The concept was successfully transferred to the current AA6082. The optimised condition (UFG-HT) that is achieved by RT processing for only one extrusion in the water quenched solid-solution temper followed by post-ECAP aging exhibits a ~30% higher strength with only ~25% reduced ductility when compared with CG-T6. The reason for the exceptional combination of high strength and moderate ductility is caused by the formation of very fine precipitates and ultrafine grains. Figure 3 shows exemplarily a STEM micrograph of this optimised microstructure. In [30] it was shown that the formation of micro shear bands plays an important role for the grain refinement of AA6063T6 during the first extrusions of a billet. Figure 3 shows such a micro shear band (width ~800 nm) containing equiaxed grains with an average size in the range of ~100 to ~300 nm. According to the results of [6, 31, 32], the predominant needle-shaped precipitate phase in the surrounding elongated cellular matrix can be associated to β'' particles. It is assumed that the strength increase during aging can be associated to the precipitation activity, while simultaneous acting recovery based on annihilation and arrangement of dislocations restores the ductility [29, 33]. Thus, the tensile properties of the UFG-HT condition engage an intermediate position between the CG-T6 and the UFG-E8 condition.

In Fig. 2b load displacement curves received of Charpy impact tests are presented. The area covered by the curves

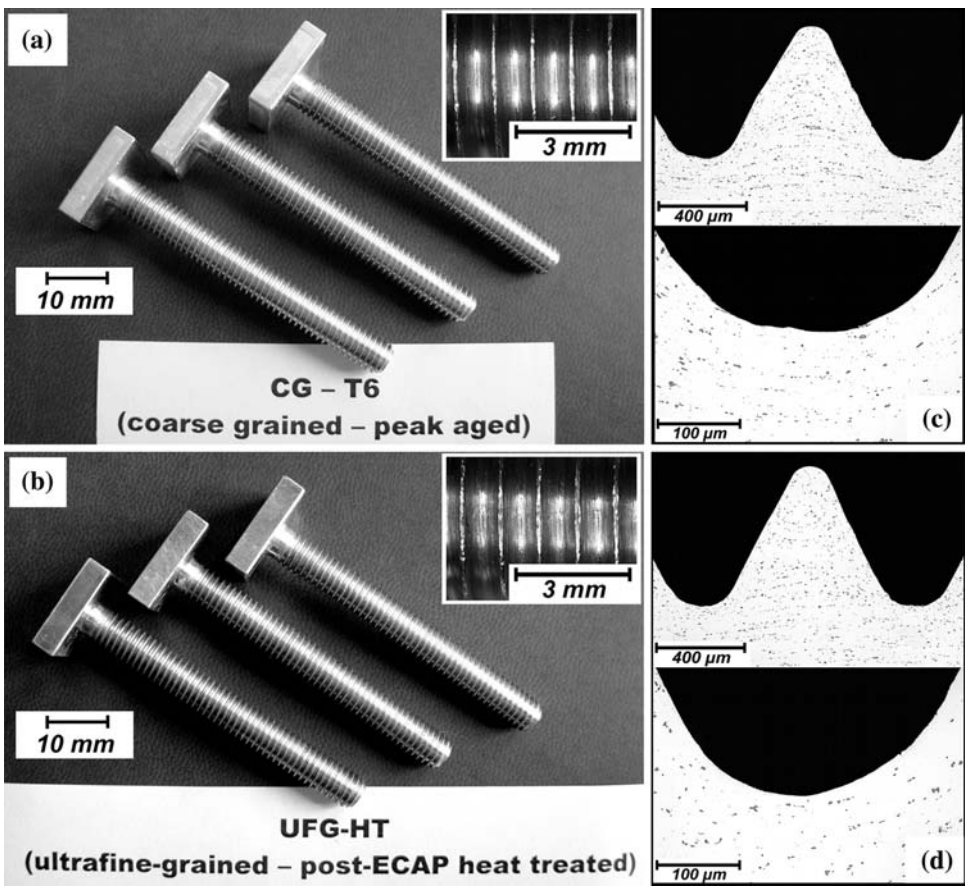

Fig. 4 Screw prototypes (M6 × 50) produced by flat-die thread rolling for (**a**) CG-T6 and (**b**) UFG-HT and micrographs of threads for (**c**) CG-T6 and (**d**) UFG-HT

Table 1 Mechanical properties of the investigated AA6082 (a) for the materials and (b) for the screws

	Tensile test								Charpy test	
	YS (MPa)	YS_{rel}	UTS (MPa)	UTS_{rel}	UEL (%)	UEL_{rel}	EL (%)	EL_{rel}	KV (J)	KV_{rel} (J)
(a)										
CG-T6	231 ± 2	1.00	269 ± 3	1.00	8.9 ± 0.3	1.00	24.5 ± 0.1	1.00	1.93 ± 0.08	1.00
UFG-E2	379 ± 3	1.64	385 ± 3	1.43	0.7 ± 0.1	0.08	14.8 ± 0.7	0.60	1.18 ± 0.16	0.61
UFG-E8	405 ± 3	1.75	419 ± 1	1.56	0.9 ± 0.1	0.10	17.2 ± 1.0	0.70	1.18 ± 0.09	0.61
UFG-HT	312 ± 4	1.35	343 ± 0	1.28	6.7 ± 0.3	0.75	17.9 ± 2.6	0.73	1.45 ± 0.13	0.75
(b)										
CG-T6	309 ± 3	1.00	334 ± 2	1.00	3.4 ± 0.2	1.00	8.7 ± 0.6	1.00		
UFG-HT	322 ± 12	1.04	363 ± 2	1.09	4.4 ± 0.3	1.29	10.1 ± 0.5	1.16		

Note: YS, yield stress at 0.2% plastic strain; UTS, ultimate tensile stress; UEL, uniform elongation; EL, elongation to failure; rel, value/value CG-T6

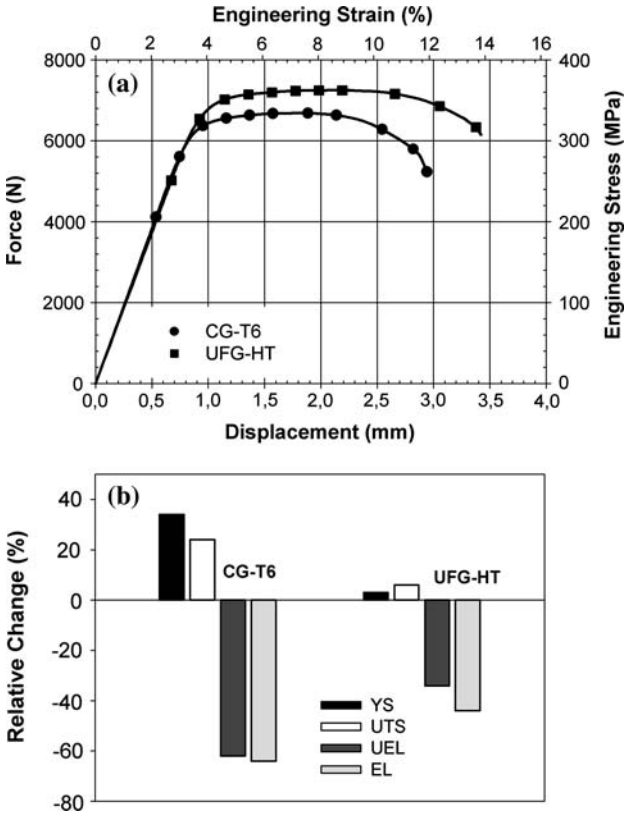

Fig. 5 Mechanical behaviour of the AA6082 screw prototypes: (**a**) force–displacement curves at quasi-static tensile loading; (**b**) relative change in mechanical properties due to the rolling of the threads calculated by $(Value_{Screw}/Value_{Material}) - 1$. YS, yield stress at 0.2% plastic strain; UTS, ultimate tensile stress; UEL, uniform elongation; EL, elongation to failure

corresponds to the absorbed energy while the progression of the curve gives information about the crack propagation. The maximum forces as well as the displacements are in good correlation with the strength and ductility from the tensile tests. The absorbed energy of the CG-T6 material is 1.9 J. After ECAP the impact toughness decreases for

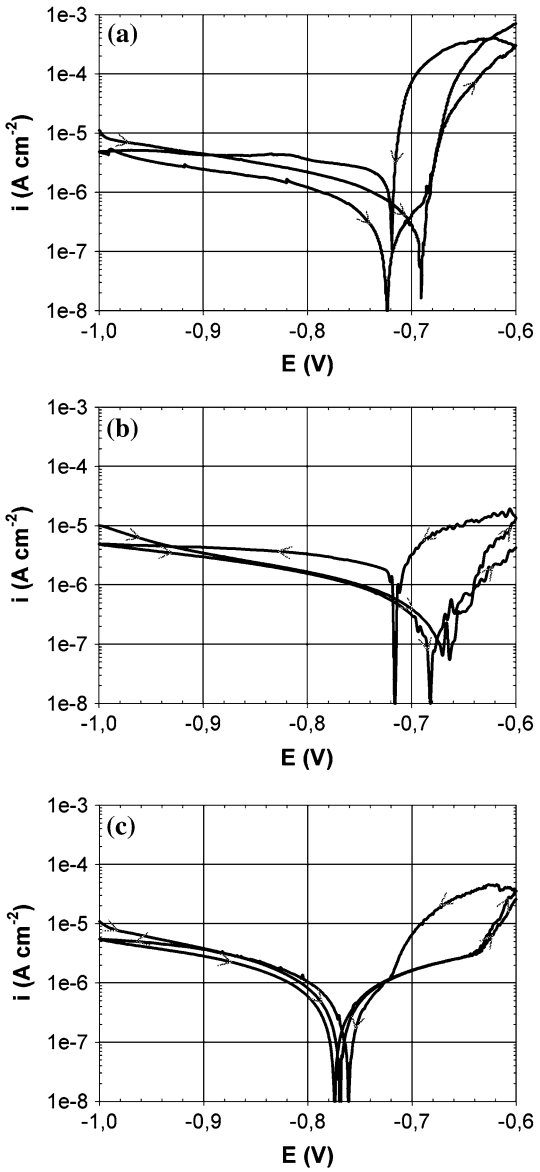

Fig. 6 Effect of ECAP and heat treatment on CV curves of AA6082 (**a**) CG-T6, (**b**) UFG-E8 and (**c**) UFG-HT

~40% since the energy absorbed during crack propagation is strongly reduced, which is indicated by the abrupt drop after crack formation. It is worth mentioning that the fracture behaviour was found to be still ductile since no indications for cleavage were detected on the fracture surfaces. Similar to the tensile tests, the application of ECAP combined with heat treatment enables the generation of an intermediate behaviour that reaches ~60% of the initial impact toughness and shows considerable stable crack propagation.

Due to the combination of high strength with moderate ductility and impact toughness, UFG-HT was selected for the production of screw prototypes. CG-T6 was investigated for reference purpose. As shown in Fig. 4a and d, there is no difference in quality of the threads visible on the macroscopic scale. In terms of mechanical performance, the roots, corresponding to the minor diameter of the thread, are the most important quality criterion for screws, especially for applications with cyclic loading. From the micrographs in Fig. 4 it is apparent that for both conditions neither at the roots nor at the crests rolling induced cracks were formed. Quasi-static tensile tests were performed on the screws for the characterisation of their stress–strain response. The results, which show a very good reproducibility and low standard deviation, are presented in Table 1. Matching force–displacement curves are shown in Fig. 5a, where a clear improvement was found for the screws made from the ECA-processed material. A maximum force of 7300 N corresponding to a stress of 363 MPa is reached. This value is ~10% higher compared to the screws made from the CG-T6 and ~15% above the value required in the standard covering the mechanical properties of fasteners made from nonferrous metals (DIN EN 28839). The minimum strain to failure is exceeded for ~45%. The changes in mechanical properties due to the cold rolling of the threads are displayed in Fig. 5b. Accordingly, the CG-T6 material undergoes a significant strain hardening, which is expressed by the increase in strength of ~30% and a considerable reduction of ductility for ~60%. For the UFG-HT material the influence of cold rolling is less pronounced indicated by the clearly lower increase in strength and also much lower ductility reduction.

Table 2 Corrosion characteristics of AA6082

	E_{pit} (mV)	E_{corr} (mV)	i_{corr} (A cm^{-2})
CH-T6	−687	−691	1.23E-06
UFG-E8	−632	−664	8.91E-07
UFG-HT	−631	−717	1.40E-06

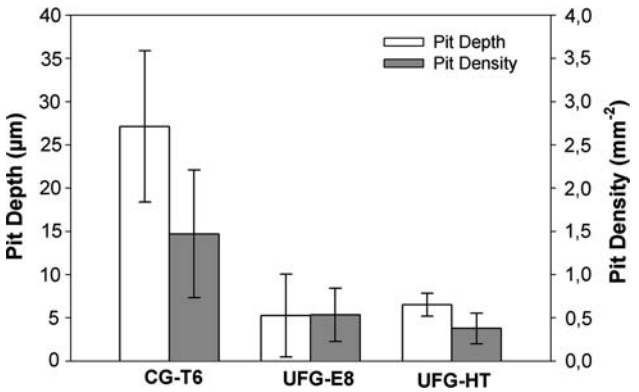

Fig. 7 The effect of ECAP on pit depth and pit density

Corrosion properties

The corrosion properties of the AA6082 were investigated for the as-received condition (CG-T6), for the UFG condition after eight ECA-extrusions (UFG-E8) as well as for the optimised condition (UFG-HT). Figure 6 shows the typical potentiodynamically registered CV curves. It is obvious that the polarization curves of all specimens are qualitatively similar. The individual corrosion characteristics are given in Table 2. The deviation of the corrosion potential E_{corr} and the corrosion current density i_{corr} are insignificant and within the experimental scatter, since at least three measurements of each condition were performed. The natural oxide film on aluminium and its alloys generally hinders the inherently active behaviour of this metal. However, solutions containing aggressive anions such as Cl^- cause pit initiation, resulting in a rapid increase of the current density at a certain potential. E_{pit}

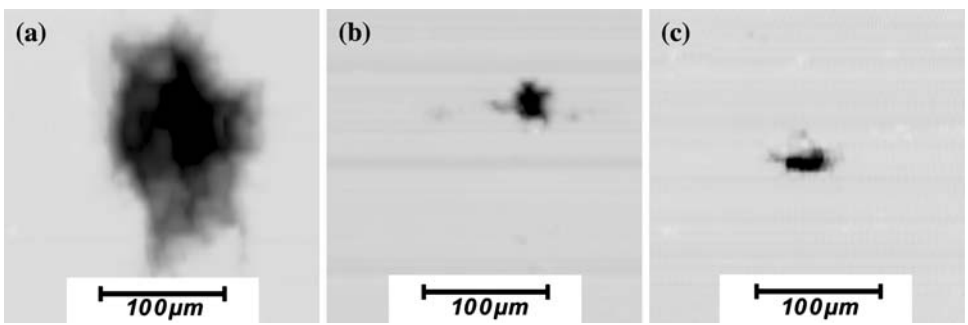

Fig. 8 The lateral extent of the largest pits for (**a**) CG-T6, (**b**) UFG-E8 and (**c**) UFG-HT

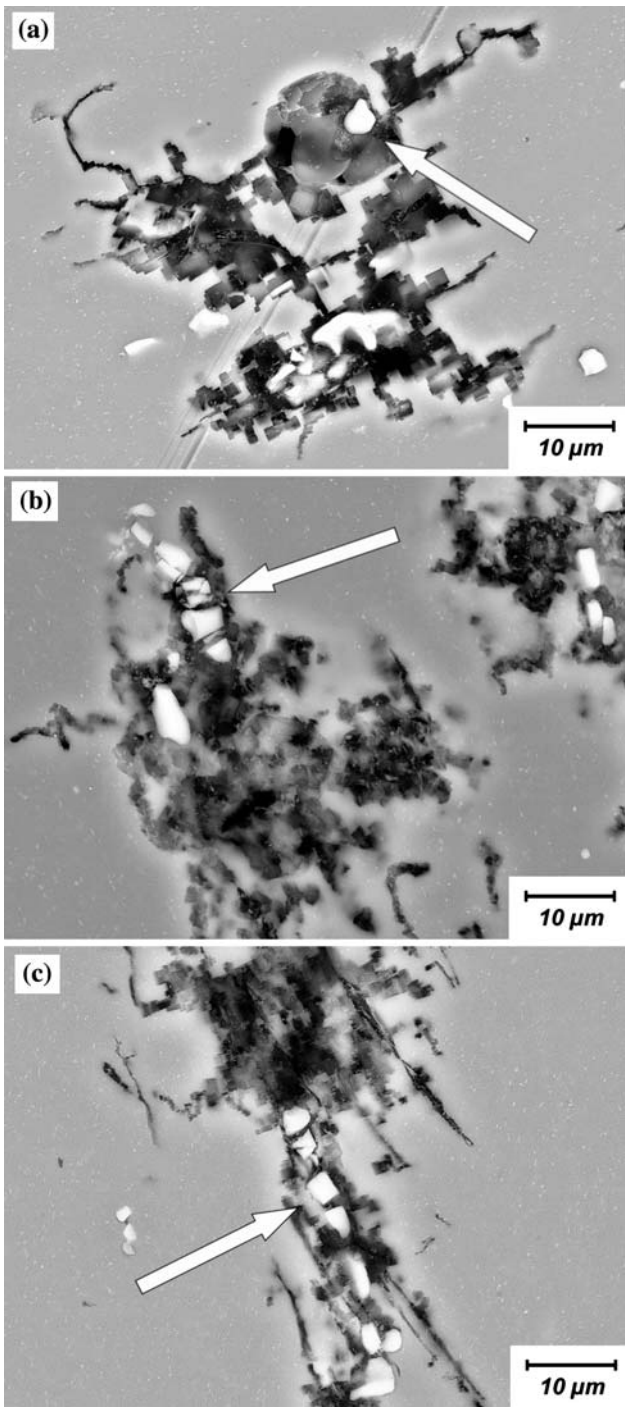

Fig. 9 SEM micrographs of the distribution of the second phases in the Al matrix and the appearance of the pits (arrows mark $Al_x(MgSiMnFe)_y$) in (**a**) CG-T6, (**b**) UFG-E8 and (**c**) UFG-HT

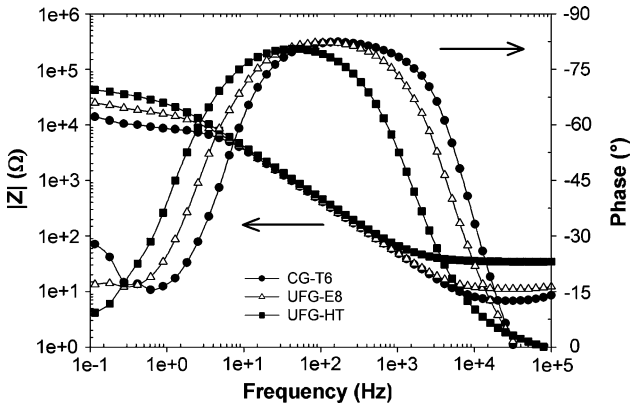

Fig. 10 Bode plot for AA6082 for the investigated conditions

characterising the breakdown of the passive film is shifted to the more noble direction by ECAP.

Thus, it can be concluded that there is no qualitative difference in the general corrosion characteristics, as it is indicated by the similar pitting corrosion behaviour. However, an evident quantitative variation in the pit initiation and propagation is expressed by the increased E_{pit} through ECAP as well as post-ECAP aging. Hence, the pitting corrosion resistance is increased by ECA-processing.

A broad description of the corrosion characteristics requires the exploration of the surface with emphasis on the corrosion damage induced. In an innovative method, the degree of localized corrosion damage was quantified by 3D-topography measurements using pit depth and pit density as characteristic parameters. Figure 7 reveals that both pitting density and depth are reduced. Besides the evident effect of ECAP on the pitting corrosion damage of CG-T6 and UFG-E8, the standard deviation of these parameters is considerably reduced for UFG-HT which is attributed to a modified distribution of the microstructural inhomogeneities. This is caused by the different thermo-mechanical history. The CG-T6 counterpart exhibits the deepest pits with 40 µm, whereas UFG-E8 and UFG-HT exhibit maximum pit depths of 14 and 8 µm, respectively. The same ranking can be deduced concerning the extent of the damage by 3D-investigations shown in Fig. 8. For this purpose the largest damage on the samples surface was captured.

Preferential pitting corrosion near the Fe-, Mn- and Si-rich impurities identified by EDXS is seen on the surfaces of all specimens (Fig. 9), suggesting that these are the most critical sites for pit initiation owing to the highest difference of the potentials. Affected by ECAP, the impurities are fragmented and more homogeneously distributed. This results in fine dispersed anodic-cathodic districts. As a consequence, pits with smaller lateral extent are formed in the matrix, as the pit initiation is retarded. Hence, the microgalvanic currents of the induced reactions proposed by [15] for Al 99.5 are reduced also in the present Al-alloy as shown by the corrosion attacks on the sample surface as well as in the more narrow crystallographic corrosion channels. We assume that the reduced size and more homogeneous distribution of impurities form smaller

corrosion elements on the one hand and lead to a more stable oxide layer also retarding the corrosion attack on the other hand. However, despite the different thermo-mechanical history, the same tendency was found for UFG-HT. The morphology of the pitted area of UFG-HT is changed, Fig. 9c. Therefore the structural influence on the pit propagation is obvious. In contrast, the pitted area of UFG-E8 in Fig. 9b appears more compact and homogenous as result of eight ECA-extrusions.

Additionally, the polarization resistance R_p for the corrosion reaction was determined by means of EIS measurements at the corrosion potential to assure anodic and cathodic reactions. Figure 10 presents the Bode plot including the impedance and phase data for AA6082 in the different conditions. There is a tendency of increased R_p after ECAP in the peak aged condition (UFG-E8) as well as after ECAP in the solid-solution heat treated condition followed by short time aging (UFG-HT). This enhanced R_p can be dedicated to a more homogeneous Al oxide layer with reduced defect size, which is presumably responsible for the comprising corrosion behaviour of UFG Al alloys compared to the CG material.

Conclusion

RT-ECAP was applied on the commercial AA6082 up to eight extrusions in a die with an internal angle of 90° following Route E with active backpressure. Besides the peak-aged temper, which gave maximum strength and a strongly reduced ductility, the solid-solution heat treated condition combined with post-ECAP aging was considered as well. With this approach a combination of high strength with moderate ductility and impact toughness was achieved. This optimised condition was consecutively used for the production of screw prototypes by flat-die thread rolling. An appreciable higher strength (~10%) and ductility (~30%) was achieved when compared to the identical manufactured screws from the CG counter material. Besides the mechanical properties, the corrosion behaviour represents a crucial feature for practical application of fasteners. It can be concluded that commercially multiphase materials such as AA6082 containing a lot of impurities show a slightly better corrosion resistance (e.g., E_{pit}, R_p) after ECAP and a reduced corrosion damage compared with the CG counterpart. The results demonstrate the potential for combining ECAP with an appropriate heat treatment for commercial Al–Mg–Si Al alloys to achieve superior mechanical and corrosive properties. Such materials are promising to be used for several engineering applications such as high-strength screws even at elevated temperatures.

Acknowledgements The authors gratefully acknowledge the Deutsche Forschungsgemeinschaft (DFG) for supporting this work carried out within the framework of Sonderforschungsbereich 692 (Collaborative Research Center; A2, B2). The authors would like to thank Dr. Harry Podlesak for performing the STEM investigations.

References

1. Segal VM, Reznikov AE, Drobyshevskiy AE, Kopylov VI (1981) Russ Metall 7 (English translation)
2. Valiev RZ, Langdon TG (2006) Prog Mater Sci 51:881. doi:10.1016/j.pmatsci.2006.02.003
3. Horita Z, Fujinami T, Nemoto M, Langdon TG (2000) Metall Mater Trans A Phys Metall Mater Sci 31:691. doi:10.1007/s11661-000-0011-8
4. Horita Z, Ohashi K, Fujita T, Kaneko K, Langdon TG (2005) Adv Mater 17:1599. doi:10.1002/adma.200500069
5. Liu M, Roven HJ, Yu Y, Werenskiold JC (2008) Mater Sci Eng A 483–484:59. doi:10.1016/j.msea.2006.09.144
6. Roven HJ, Liu M, Werenskiold JC (2008) Mater Sci Eng A 483–484:54. doi:10.1016/j.msea.2006.09.142
7. Ferrasse S, Segal VM, Alford F, Kardokus J, Strothers S (in press) Mater Sci Eng A
8. Friedrich C (2004) Reliable lightweight fastening of magnesium components in automotive applications. In: SAE World Congress & Exhibition, SAE Technical Papers, Detroit, MI, March 2004
9. Valiev RZ, Islamgaliev RK, Alexandrov IV (2000) Prog Mater Sci 45:103. doi:10.1016/S0079-6425(99)00007-9
10. Vinogradov A, Mimaki T, Hashimoto S, Valiev R (1999) Scr Mater 41:319. doi:10.1016/S1359-6462(99)00170-0
11. Balyanov A, Kutnyakova J, Amirkhanova NA, Stolyarov VV, Valiev RZ, Liao XZ et al (2004) Scr Mater 51:225. doi:10.1016/j.scriptamat.2004.04.011
12. Akiyama E, Zhang Z, Watanabe Y, Tsuzaki K (2007) J Solid State Electrochem 1–6
13. Hadzima B, Janecek M, Hellmig RJ, Kutnyakova Y, Estrin Y (2006) Mater Sci Forum 503–504:883
14. Vinogradov A, Miyamoto H, Mimaki T, Hashimoto S (2002) Ann Chim 27:65. doi:10.1016/S0151-9107(02)80008-3
15. Chung M-K, Choi Y-S, Kim J-G, Kim Y-M, Lee J-C (2004) Mater Sci Eng A 366:282. doi:10.1016/j.msea.2003.08.056
16. Son IJ, Nakano H, Oue S, Kobayashi S, Fukushima H, Horita Z (2006) Mater Trans 47:1163. doi:10.2320/matertrans.47.1163
17. Wei W, Wei KX, Du QB (2007) Mater Sci Eng A 454–455:536. doi:10.1016/j.msea.2006.11.063
18. Segal VM (2004) Mater Sci Eng A 386:269
19. Furukawa M, Horita Z, Langdon TG (2002) Mater Sci Eng A 332:97. doi:10.1016/S0921-5093(01)01716-6
20. Barber RE, Dudo T, Yasskin PB, Hartwig KT (2004) Scr Mater 51:373. doi:10.1016/j.scriptamat.2004.05.022
21. Cheng S, Zhao YH, Zhu YT, Ma E (2007) Acta Mater 55:5822. doi:10.1016/j.actamat.2007.06.043
22. Wang YM, Ma E, Valiev RZ, Zhu YT (2004) Adv Mater 16:328. doi:10.1002/adma.200305679
23. Zhao YH, Liao XZ, Cheng S, Ma E, Zhu YT (2006) Adv Mater 18:2280. doi:10.1002/adma.200600310
24. Zhao YH, Liao XZ, Jin Z, Valiev RZ, Zhu YT (2004) Acta Mater 52:4589. doi:10.1016/j.actamat.2004.06.017
25. Kim WJ, Kim JK, Kim HK, Park JW, Jeong YH (2008) J Alloy Compd 450:222
26. Kim JK, Jeong HG, Hong SI, Kim YS, Kim WJ (2001) Scr Mater 45:901. doi:10.1016/S1359-6462(01)01109-5

27. Kim JK, Kim HK, Park JW, Kim WJ (2005) Scr Mater 53:1207. doi:10.1016/j.scriptamat.2005.06.014
28. Kim WJ, Chung CS, Ma DS, Hong SI, Kim HK (2003) Scr Mater 49:333. doi:10.1016/S1359-6462(03)00260-4
29. Hockauf M, Meyer LW, Zillmann B, Hietschold M, Schulze S, Krüger L. Mater Sci Eng A (accepted for publication)
30. Hockauf M, Meyer LW, Halle T, Kuprin C, Hietschold M, Schulze S et al (2006) Int J Mater Res 97:1392
31. Matsuda K, Naoi T, Fujii K, Uetani Y, Sato T, Kamio A et al (1999) Mater Sci Eng A 262:232. doi:10.1016/S0921-5093(98)00962-9
32. Chakrabarti DJ, Laughlin DE (2004) Prog Mater Sci 49:389. doi:10.1016/S0079-6425(03)00031-8
33. Kim WJ, Wang JY (2007) Mater Sci Eng A 464:23. doi:10.1016/j.msea.2007.03.074